Published in final edited form as:
J Vasc Interv Radiol. 2012 February ; 23(2): 257–64.e4. doi:10.1016/j.jvir.2011.10.019.

Radiopaque Drug-Eluting Beads for Transcatheter Embolotherapy: Experimental study of Drug Penetration and Coverage in Swine

Matthew R. Dreher[1,*], **Karun V. Sharma**[1,2,*], **David L. Woods**[1], **Goutham Reddy**[1], **Yiqing Tang**[3], **William F. Pritchard**[4], **Oscar A. Chiesa**[4], **John W. Karanian**[4], **Juan A. Esparza**[4], **Danielle Donahue**[1], **Elliot B. Levy**[1], **Sean L. Willis**[3], **Andrew L. Lewis**[3], and **Bradford J. Wood**[1]

[1]Center for Interventional Oncology, Radiology and Imaging Sciences, Clinical Center & National Cancer Institute National Institutes of Health, Bethesda, MD

[2]Georgetown University Hospital, Department of Radiology, Washington DC

[3]Biocompatibles UK Ltd, Farnham Business Park, Weydon Lane, Farnham, Surrey, GU9 8QL, UK

[4]Food and Drug Administration, Center for Devices and Radiological Health, Laurel, MD

Abstract

Purpose—The *objective* of this study was to determine local doxorubicin levels surrounding radiopaque drug-eluting beads (DEB) in normal swine liver and kidney following transcatheter arterial chemoembolization (TACE). The influence of bead size (70–150μm or 100–300μm) was compared with regard to tissue penetration and spatial distribution of the bead as well as eventual drug coverage (i.e., amount of tissue exposed to drug).

Materials and Methods—Radiopaque DEBs were synthesized by suspension polymerization followed by incorporation of iodized oil and doxorubicin. Chemoembolization of swine liver and kidney was performed under fluoroscopic guidance. Three dimensional tissue penetration of image-able DEB was investigated ex vivo with microCT. Drug penetration from the bead surface and drug coverage was evaluated with epi-fluorescence microscopy while cellular localization of doxorubicin was evaluated with confocal microscopy. Necrosis was evaluated with H&E.

Results—MicroCT demonstrated that 70–150μm DEB were present in more distal arteries and located in a more frequent and homogeneous spatial distribution. Tissue penetration of doxorubicin from the bead appeared similar (~300μm) for both DEBs with a maximum tissue drug

Address correspondence to B.J.W.; bwood@nih.gov.
*MRD and KVS contributed equally

This work was presented at Society of Interventional Radiology Annual Meeting in Tampa Florida, March 13 – 18, 2010. The mention of commercial products, their source, or their use in connection with material reported herein is not to be construed as either an actual or implied endorsement of such products by the U.S. Food and Drug Administration, the National Institutes of Health, the Department of Health and Human Services or the Public Health Service.

Conflicts:
Research support was provided from biocompatibles to BJW and MRD.
ALL, SLW and YT are paid employees of Biocompatibles.

concentration at 1hr coinciding with nuclear localization of doxorubicin. The greater spatial frequency of the 70–150μm DEBs resulted in ~2-fold improved drug coverage in kidney. Cellular death is predominantly observed around the DEBs beginning at 8 hr but increased at 24 and 168 hrs.

Conclusions—Smaller DEBs penetrated further into targeted tissue (macroscopic) with a higher spatial density, resulting in greater and more uniform drug coverage (microscopic) in swine.

INTRODUCTION

Transcatheter arterial chemoembolization (TACE) is a standard treatment option for patients with unresectable primary hepatocellular carcinoma (HCC) and used to treat some liver metastases (1–3). Despite the widespread use and success of TACE for over three decades, there remains a lack of consensus regarding optimal technique (4). For example, there is variability in 1) type and size of embolic agent, 2) type and amount of chemotherapeutic agent(s), 3) degree of catheter selectivity, and 4) optimal embolization endpoint (5–8). This material and technical variability may be perpetuated by a lack of knowledge concerning the influence of these TACE variables on patient outcomes. Educated recommendations to standardize material choice and procedural technique may be formulated, if embolic material and drug locations inside the embolized tissue were known with a high degree of confidence.

The emerging use of drug-eluting beads (DEBs), in which a uniform embolic material and drug are delivered in a single image-guided step, may begin to simplify and standardize TACE (9–11). This simplification is accomplished by embolization of preloaded embolic beads that elute drug in a controlled and predictable manner once localized in the targeted tissue. Several clinical reports have suggested the benefit and safety of DEB-TACE (12–16). In contrast to “conventional” TACE, DEB-TACE lacks the intraprocedural imaging feedback of lipiodol deposition in the target tumor which is seen with fluoroscopy or CT. In order to address this lack of feedback, investigators have developed image-able beads that can be visualized with magnetic resonance (17–20) and fluoroscopic imaging (21–22) or both (23). Knowledge of bead distribution during a procedure may provide useful real-time feedback to modify the intervention and tailor the procedure to a specific patient. This approach combines one of the main advantages of conventional TACE (image-ability of lipiodol) with the uniformity and predictable drug elution of DEBs.

The ability to image beads in clinical practice may prove valuable to report on embolic location, and since the chemotherapeutics (e.g., doxorubicin and irinotecan) are initially held by the bead, imaging bead location may also serve as a surrogate for local drug levels, or at least for the location of the drug source. Drug levels within a tumor following DEB-TACE are known to be dynamic (24). Laurent and coworkers have documented drug distribution in swine liver (25) and resected liver tumor tissue (26) following DEB-TACE. The drug concentration was greatest around the beads and extended up to 600μm suggesting the ability to use an image-able drug-eluting bead as a surrogate for local drug quantification and localization.

The *objective* of this study was to determine local doxorubicin levels surrounding radiopaque doxorubicin-eluting beads in normal swine liver and kidney. To demonstrate the ability to address material variability in DEB-TACE, small (70–150μm) and more widely used (100–300μm) beads were compared with regards to spatial distribution and drug coverage. We hypothesized that smaller beads would penetrate to more distal locations and yield more uniform, homogenous, and greater drug coverage. The bead distribution was evaluated with microCT and drug distribution quantified with fluorescence microscopy of doxorubicin.

MATERIALS AND METHODS

Preparation of Lipiodol- and Doxorubicin-loaded PVA beads

The 100–300 μm LC™/DC Bead® and a specially-made 70–150 μm range version of this product (Biocompatibles UK Ltd., Farnham, UK) were used in this study (9–10). The 70–150 μm beads are simply a smaller size fraction of the 100–300 μm beads. All reagents used for loading were of analytical grade. Beads (50 mg) were lyophilized in the presence of an excipient (Mannitol) and then mixed with 1 mL of Lipiodol (Guerbet, France). All beads were loaded with 37.5mg of doxorubicin in 1 mL of beads. Characterization of radiopaque drug eluting beads including size and elution was performed with standard technique. Additional details may be found in supplemental information.

Transcatheter chemoembolization of swine liver and kidney with radiopaque drug-eluting beads

This manuscript was written with terminology and reporting standards of the Society of Interventional Radiology (4). All animal studies were conducted under an animal use protocol approved by an Institutional Animal Care and Use Committee. The ability to visualize radiopaque DEBs was evaluated *in vivo* with routine fluoroscopy and CT during DEB-TACE in normal swine liver and kidney. Additional details may be found in supplemental information. Briefly, the procedure was performed in a CT/angiography suite in which a 16 slice CT was combined with a C-arm. Domestic swine (n=9) with weights close to that of human patients (mean = 72kg, range = 66–84kg) were used to ensure relevant sized anatomical structures. Following induction of anesthesia, animals were intubated and maintained under general anesthesia with isoflurane. A 2.8 Fr microcatheter was then used to select lobar hepatic artery branches or branches of the main renal artery.

For liver embolizations, the catheter tip was positioned to isolate a different hepatic arterial supply (alternating between left lateral and right lateral lobar arteries). One mL of the beads was suspended in a total volume of 20–25 ml D5W and infused slowly under careful fluoroscopic monitoring. Iodinated contrast was not used for bead suspension, because one of the aims of the study was to evaluate conspicuity of the radiopaque beads themselves. The embolization endpoint was delivery of the entire dose. Branches of renal arteries were embolized in a similar manner. At the end of the study, the animals were euthanized and embolized organs were harvested at indicated time points and immediately dissected into relevant samples.

Tissue analysis

Additional details may be found in supplemental information. Briefly, high resolution three-dimensional spatial distribution of radiopaque drug-eluting beads within swine liver and kidney after DEB-TACE was determined with microCT. Semi-quantitative analysis of doxorubicin distribution following embolization of swine liver was performed by comparing fluorescence intensity between tissue images and that of known standards of doxorubicin. Drug coverage was determined by analyzing the fluorescence intensity of doxorubicin in swine kidney tissue 1 hr following embolization with radiopaque doxorubicin-eluting beads and calculated by dividing doxorubicin area by the total image area. Cellular uptake of doxorubicin was investigated with a laser scanning confocal fluorescence microscope. Hematoxylin and eosin analysis was performed in the immediate vicinity of the bead to document tissue changes.

Statistics

Statistical analyses were performed in GraphPad Prism 5 (GraphPad Software, La Jolla, CA). Comparisons between two groups were performed with a t-test. P-values less than 0.05

were considered statistically significant and all statistical tests were two-sided. Data are reported as mean ± SEM unless otherwise indicated.

RESULTS

In vitro characterization of radiopaque drug-eluting beads

Doxorubicin loaded radiopaque beads appeared similar to standard doxorubicin loaded beads that are not radiopaque, except that they settled more rapidly in a syringe. A durable suspension was obtained when the beads were hydrated in a 50:50 sterile water and contrast mixture (or greater amounts of contrast), as often used in clinical practice. The iodine content was 23.4–23.9wt% depending on batch (lipiodol = 38.2wt% iodine). As shown in Figure 1A, the radiopaque beads eluted doxorubicin slightly more slowly than non-radiopaque beads. Consistent with published data (10, 27), the smaller beads had a more rapid elution than larger beads, most likely due to the greater surface area to volume ratio of a smaller bead. The radiopaque beads were also slightly larger (180±44 or 116±13 μm, mean ±SD) than non-radiopaque (155±53 or 96±12 μm) beads (Figure 1B).

In vivo visualization of radiopaque drug-eluting beads

The ability to visualize radiopaque drug-eluting beads in vivo was evaluated with clinical fluoroscopy and CT units. Both 70–150μm and 100–300μm beads provided sufficient contrast to be observed with CT (see supplemental information) and fluoroscopy (faint appearance). The parenchymal enhancement demonstrated by transcatheter CTA with liquid iodinated contrast is entirely absent when only radiopaque beads are delivered. Instead a vascular cast appearance is obtained with radiopaque beads. The discordance between CTA images, showing iodinated contrast location, and the radiopaque bead images, showing eventual bead location, highlights both the usefulness (approximate target region) and limitations of using a transcatheter CTA to indicate eventual bead location.

Ex vivo visualization of radiopaque drug-eluting beads with microCT

Embolized liver and kidney tissue was evaluated ex vivo with microCT to investigate the true distribution of embolic beads because, in contrast to clinical CT, microCT is capable of resolving individual beads. Figure 2 demonstrates that beads formed long columns of beads with an occasional single bead or group of 1–3 beads. Multiple beads grouped across an artery diameter appeared to be required for visualization with clinical CT. 70–150μm beads penetrated further into the tissue reaching more distal locations. For example, more 70–150μm than 100–300μm beads are found near the renal capsule surface in the axial image of Figure 2. The spatial frequency or density of 70–150μm beads is much greater than 100–300μm beads, most likely due to improved accessibility of a smaller bead to the greater spatial density of small arteries in normal arterial architecture. A similar appearance was observed in liver tissue.

Doxorubicin penetration into normal swine liver tissue

The penetration of doxorubicin into liver tissue was examined with epi-fluorescent microscopy up to 1 week following embolization. Representative images for 70–150μm beads are shown in supplemental information. Initially, most of the drug is contained within the bead and diminished dramatically over 24 hours. The concentration within the tissue, indicated by fluorescence intensity, was greatest immediately surrounding the bead and declined over hundreds of microns from the bead surface. The greatest tissue drug levels appeared within the first 4 hours following embolization.

Semi-quantitative analysis of doxorubicin concentration was performed by analyzing fluorescence images as shown in supplemental information using known calibration

standards. Figure 3 demonstrates the penetration of doxorubicin over 1 week from the bead surface. Similar to the fluorescence images, doxorubicin concentration declined with distance from the bead surface. Initially 30 minutes following embolization, the drug levels are very high (~30–40 μM) adjacent to the bead surface. The overall concentration increased from 30 min to 1 hr, and remained markedly elevated up to 8 hours following embolization. After 24 hours, the concentration substantially declined to ~0.5–5.0 μM for distances up to 150 μm from the bead surface. One week following embolization, doxorubicin was still detected but the concentration was much lower.

No substantial difference was observed in the tissue concentration or penetration of doxorubicin for 70–150μm or 100–300μm beads. This is somewhat surprising as larger beads have potential to contain greater amounts of drug per bead, i.e., greater drug source with larger beads. However, this phenomenon was evident when examining groups of beads compared to a single bead. As shown in supplemental information, the tissue concentration is greater for a group of beads with an apparent increase in penetration. MicroCT analysis of the embolized tissues herein as well as histology data from other animal studies (25) and embolized human HCC livers (26) demonstrated that beads are frequently found in groups inside the arterial lumen. Therefore, the average drug concentration and apparent penetration in routine clinical practice is most likely higher than shown for a single bead in Figure 3.

Doxorubicin coverage in normal swine kidney

Drug coverage, the fraction of cells exposed to a substantial concentration of drug, was evaluated with epi-fluorescence microscopy. The bead density was often sparse or spatially infrequent in swine renal tissue, leaving large regions that are not exposed to drug. MicroCT images shown in Figure 2 suggest that smaller beads take advantage of arterial architecture and yield a more spatially homogenous and dense distribution of beads. Since doxorubicin tissue penetration is similar between 70–150μm and 100–300μm beads, the improved distribution of small beads should result in greater drug coverage. In fact, 70–150μm beads provided ~2-fold greater coverage (19.0 ± 3.1%) than 100–300μm beads (10.9 ± 2.1%, n = 31–40, p-value = 0.0301).

Intracellular doxorubicin uptake and tissue changes

Intracellular uptake and subcellular distribution of doxorubicin was evaluated with confocal microscopy, as shown in Figure 4. Doxorubicin is classically thought to act in the nucleus to induce cell death. Initially, 30 min following embolization, doxorubicin was found surrounding normal hepatocytes. Predominantly nuclear localization emerged by 1 hr following embolization and appeared to increase up to 8 hr. Cellular organization is markedly changed at 24hr and less cellularity was observed by 7 days. The higher magnification image at 8hr in Figure 4 exhibits a loss of nuclear organization. Often structures such as bile ducts, as shown at 2hr, demonstrated a high concentration of drug on the side proximal to the bead but much less drug on the distal side. This appearance suggests that the convective flow in structures such as bile ducts may act as a drug sink and alter drug distribution.

Tissue changes were evaluated with H&E, as shown in Figure 5. Peri-bead necrosis was abundant at 24 hr with the appearance of karyorrhectic nuclei. Necrosis often extended hundreds of microns, similar to the doxorubicin distribution surrounding the beads, suggesting that this cell death may be due to drug exposure. However, regions of necrosis were often identified without containing a bead. These regions of sporadic necrosis may be due to beads out of the image plane, ischemia and/or potential bystander effects.

DISCUSSION

Practical use of radiopaque drug eluting beads

Use of radiopaque drug eluting beads in DEB-TACE has the potential to provide valuable intraprocedural feedback regarding the location or completeness of treatment and to tailor the procedure to patient-specific tumor vascularity and anatomy. Although radiopaque beads have been demonstrated (21–23), the ability to load both an X-ray contrast agent (lipiodol) and drug (doxorubicin) inside the same bead with minimal effect on the drug loading (data not shown) and elution properties (see Figure 1) is a necessary step toward clinical translation.

Although somewhat instructive, comparing transcatheter CTA images with eventual bead location demonstrated a considerable discordance that depends on the phase of imaging in which the CTA images are obtained. This finding suggests that soluble contrast does not accurately depict eventual bead location. Transcatheter angiography with X-ray (28–30) or MR (31) may be better suited to evaluate perfusion changes than eventual bead location. The emerging practice of cone beam CT during TACE (28–30) may work well in combination with radiopaque drug-eluting beads. Ex vivo examination of embolized tissue demonstrated that cone beam CT may resolve more beads than conventional CT, approaching the resolution of microCT. Studies are ongoing to investigate the utility of cone beam CT during DEB-TACE with radiopaque beads which may be more clinically applicable to this strategy than fluoroscopy.

Bead and drug penetration

There are many length scales over which to consider penetration of both embolic beads and drug following DEB-TACE (32). First, the bead must be able to reach the targeted tissue, such as a tumor, within the liver. In clinical practice this is influenced by catheter selectivity. Available data from histological evaluation of resected livers suggests that only half of the beads reside in a targeted tumor versus normal liver (26). Additionally, penetration of beads into small tumor vasculature has the potential to reach more distant locations within a tumor (such as a tumor core). Once the embolic beads have reached their final location, the penetration of drug from the bead surface will depend on the drug's physicochemical characteristics, tissue properties, and the release characteristics of the drug. Bead size appears to be a dominant variable to influence penetration at all length scales.

As shown in Figure 2 smaller beads penetrated more distally, resulting in a more homogeneous distribution in the targeted tissue, yielding improved drug coverage. The limited drug coverage for 100–300μm beads (10.9%) in the well vascularized normal kidney combined with the sparsity of beads in available data from resected tumors (26) suggests that drug coverage may be significantly improved. The ~2-fold greater drug coverage with 70–150μm beads suggests that smaller beads have potential to both gain access to tumor sites previously unreachable by larger beads and provide greater drug coverage. The exact size of bead that may yield optimal clinical outcomes will most likely depend on tumor histology and size of tumor vascularity in an individual patient. Use of 25–35μm beads for radioembolization (33), 40μm for bland embolization (34) and vascular penetration measurements in preclinical models (35) all suggests that the lower limit may be ~25–50μm as serious adverse events have been reported with small beads (34, 36). It is probable that progressively smaller drug eluting beads will continue to be used, as has occurred over the last 5 years (12–16, 37), until clinical data reveals a practical or safety limitation.

Laurent and coworkers have used microspectrofluorimetry, which is a more rigorous and quantitative technique, to measure doxorubicin penetration for time periods up to 90 days (25–26). The overall shape of the penetration profile is similar to that presented herein

suggesting diffusion dominated transport. This current study examined earlier time points following DEB-TACE and demonstrated that tissue drug concentration was markedly elevated within the first 8 hrs following embolization although drug was still observed following 1 week. Drug concentration in hypervascular tumors may be higher than normal liver parenchyma due to higher bead concetration.

Tissue changes following DEB-TACE

The cause of normal and tumor cell death following DEB-TACE remains unclear but is most likely a combination of ischema and drug effects. Cell death is dependent on the duration of drug exposure as well as drug concentration (25–26). Since drug levels vary in time and location (see Figure 3), the exact exposure of doxorubicin that corresponds to tumor or normal cell death remains elusive. Despite this limitation, the distribution of peri-bead necrosis is similar to the extent of doxorubicin penetration observed over the first 24hrs. The peri-bead concentrations of doxorubicin obtained within 7 days are considered to be in the range of cytotoxic drug levels, 7.9 to 0.42 μM (25–26). In a complex tumor microenvironment, the relative contributions of drug, ischemia, and/or bystander effect (i.e., cell death resulting from death of vital nearby cells) will be hard to differentiate. Since doxorubicin is largely confined to a few hundred microns of the bead surface, imaging the bead may be able to report on local tissue drug levels and distribution.

This study has several limitations. The normal swine animal model is useful because of the relevant sized vascular anatomy, but is limited by a lack of tumor. Future studies in a Vx2 animal tumor model (38–40) or clinical trials, with variable vascularity and necrosis as found in patients with HCC, are better suited to evaluate the real utility of radiopaque drug-eluting beads. Even under the most controlled circumstances, fluorescence measurements of drug concentration may be considered only semi-quantitative since the local environment of the fluorophore may influence its observed intensity.

The use of radiopaque DEBs may provide valuable intraprocedural feedback to report on embolic and drug location, which may have important consequences. First, the use of radiopaque beads as a research tool may provide essential information to reduce material choice and technical variability and formulate educated recommendations on a more standard practice of TACE. Second, knowledge of embolic and drug location can be used in more rational combination therapy with systemic and/or local-regional approaches. For example, ablation with needles or antennae can be targeted towards areas with less drug or bead distribution. Finally, personalized medicine can be fostered through individually-tailored drug delivery that is specific to each patient.

Smaller DEBs take advantage of arterial anatomy, penetrating further into targeted tissue (macroscopic) with a higher spatial density, resulting in greater and more uniform drug coverage (microscopic). The use of radiopaque drug-eluting beads may provide valuable intraprocedural feedback to report on embolic and drug location.

Supplementary Material

Refer to Web version on PubMed Central for supplementary material.

Acknowledgments

This study was conducted in the Center for Interventional Oncology and is supported in part by the Intramural Research Program of the National Institutes of Health (NIH), the Society of Interventional Radiology Foundation Ring Grant, and an Interagency Agreement between the NIH and the United States Food and Drug Administration (FDA). NIH and Biocompatibles, Ltd. have a Cooperative Research and Development Agreement. We thank the

Ankur Kapoor for advice on image processing and the Mouse Imaging Facility of NIH for assistance with micro-CT.

ABREVIATIONS

DEBs	Drug eluting beads
TACE	Transarterial chemoembolization
HCC	Hepatocellular carcinoma
CTA	computed tomographay angiography

REFERENCES

1. Llovet JM, Real MI, Montana X, et al. Arterial embolisation or chemoembolisation versus symptomatic treatment in patients with unresectable hepatocellular carcinoma: a randomised controlled trial. The Lancet. 2002; 359(9319):1734–1739.
2. Lo CM, Ngan H, Tso WK, et al. Randomized controlled trial of transarterial lipiodol chemoembolization for unresectable hepatocellular carcinoma. Hepatology. 2002; 35(5)
3. Liapi E, Geschwind JF. Transcatheter arterial chemoembolization for liver cancer: is it time to distinguish conventional from drug-eluting chemoembolization? Cardiovasc Intervent Radiol. 2011; 34(1):37–49. [PubMed: 21069333]
4. Brown DB, Gould JE, Gervais DA, et al. Transcatheter therapy for hepatic malignancy: standardization of terminology and reporting criteria. J Vasc Interv Radiol. 2007; 18(12):1469–1478. [PubMed: 18057279]
5. Brown DB, Geschwind JFH, Soulen MC, Millward SF, Sacks D. Society of Interventional Radiology position statement on chemoembolization of hepatic malignancies. J Vasc Interv Radiol. 2006; 17(2P1):217–223. [PubMed: 16517767]
6. Geschwind JFH, Ramsey DE, van der Wal BCH, et al. Transcatheter arterial chemoembolization of liver tumors: effects of embolization protocol on injectable volume of chemotherapy and subsequent arterial patency. Cardiovasc Intervent Radiol. 2003; 26(2):111–117. [PubMed: 12616414]
7. Brown DB, Pilgram TK, Darcy MD, et al. Hepatic arterial chemoembolization for hepatocellular carcinoma: comparison of survival rates with different embolic agents. J Vasc Interv Radiol. 2005; 16(12):1661–1666. [PubMed: 16371533]
8. Lewandowski RJ, Wang D, Gehl J, et al. A comparison of chemoembolization endpoints using angiographic versus transcatheter intraarterial perfusion/MR imaging monitoring. J Vasc Interv Radiol. 2007; 18(10):1249–1257. [PubMed: 17911515]
9. Lewis AL. DC Bead(TM): a major development in the toolbox for the interventional oncologist. Expert Rev Med Devices. 2009; 6(4):389–400. [PubMed: 19572794]
10. Lewis AL, Gonzalez MV, Lloyd AW, et al. DC bead: in vitro characterization of a drug-delivery device for transarterial chemoembolization. J Vasc Interv Radiol. 2006; 17(2 Pt 1):335–342. [PubMed: 16517780]
11. Taylor RR, Tang Y, Gonzalez MV, Stratford PW, Lewis AL. Irinotecan drug eluting beads for use in chemoembolization: in vitro and in vivo evaluation of drug release properties. Eur J Pharm Sci. 2007; 30(1):7–14. [PubMed: 17030118]
12. Varela M, Real MI, Burrel M, et al. Chemoembolization of hepatocellular carcinoma with drug eluting beads: efficacy and doxorubicin pharmacokinetics. J Hepatol. 2007; 46(3):474–481. [PubMed: 17239480]
13. Poon RTP, Tso WK, Pang RWC, et al. A Phase I/II Trial of Chemoembolization for Hepatocellular Carcinoma Using a Novel Intra-Arterial Drug-Eluting Bead. Clinical Gastroenterology and Hepatology. 2007; 5(9):1100–1108. [PubMed: 17627902]
14. Malagari K, Chatzimichael K, Alexopoulou E, et al. Transarterial Chemoembolization of Unresectable Hepatocellular Carcinoma with Drug Eluting Beads: Results of an Open-Label Study of 62 Patients. Cardiovasc Intervent Radiol. 2008; 31:269–280. [PubMed: 17999110]

15. Reyes DK, Vossen JA, Kamel IR, et al. Single-center phase II trial of transarterial chemoembolization with drug-eluting beads for patients with unresectable hepatocellular carcinoma: initial experience in the United States. Cancer J. 2009; 15(6):526–532. [PubMed: 20010173]

16. Lammer J, Malagari K, Vogl T, et al. Prospective randomized study of doxorubicin-eluting-bead embolization in the treatment of hepatocellular carcinoma: results of the PRECISION V study. Cardiovasc Intervent Radiol. 2010; 33(1):41–52. [PubMed: 19908093]

17. Gupta T, Virmani S, Neidt TM, et al. MR tracking of iron-labeled glass radioembolization microspheres during transcatheter delivery to rabbit VX2 liver tumors: feasibility study. Radiology. 2008; 249(3):845–854. [PubMed: 18840788]

18. Lee KH, Liapi E, Vossen JA, et al. Distribution of iron oxide-containing Embosphere particles after transcatheter arterial embolization in an animal model of liver cancer: Evaluation with MR Imaging and implication for therapy. J Vasc Interv Radiol. 2008; 19(10):1490–1496. [PubMed: 18755602]

19. Namur J, Chapot R, Pelage JP, et al. MR imaging detection of superparamagnetic iron oxide loaded tris-acryl embolization microspheres. J Vasc Interv Radiol. 2007; 18(10):1287–1295. [PubMed: 17911520]

20. Wilson MW, Fidelman N, Weber OM, et al. Experimental renal artery embolization in a combined MR imaging/angiographic unit. J Vasc Interv Radiol. 2003; 14(9 Pt 1):1169–1175. [PubMed: 14514809]

21. Sharma KV, Dreher MR, Tang Y, et al. Development of "imageable" beads for transcatheter embolotherapy. J Vasc Interv Radiol. 2010; 21(6):865–876. [PubMed: 20494290]

22. Saralidze K, van Hooy-Corstjens CS, Koole LH, Knetsch ML. New acrylic microspheres for arterial embolization: combining radiopacity for precise localization with immobilized thrombin to trigger local blood coagulation. Biomaterials. 2007; 28(15):2457–2464. [PubMed: 17257667]

23. Bartling SH, Budjan J, Aviv H, et al. First multimodal embolization particles visible on x-ray/computed tomography and magnetic resonance imaging. Invest Radiol. 2011; 46(3):178–186. [PubMed: 21263332]

24. Hong K, Khwaja A, Liapi E, Torbenson MS, Georgiades CS, Geschwind JFH. New intra-arterial drug delivery system for the treatment of liver cancer: preclinical assessment in a rabbit model of liver cancer. Clin Cancer Res. 2006; 12(8):2563. [PubMed: 16638866]

25. Namur J, Wassef M, Millot JM, Lewis AL, Manfait M, Laurent A. Drug-eluting beads for liver embolization: concentration of doxorubicin in tissue and in beads in a pig model. J Vasc Interv Radiol. 2010; 21(2):259–267. [PubMed: 20123210]

26. Namur J, Citron SJ, Sellers MT, et al. Embolization of hepatocellular carcinoma with drug-eluting beads: doxorubicin tissue concentration and distribution in patient liver explants. J Hepatol. 2011

27. Lewis AL, Taylor RR, Hall B, Gonzalez MV, Willis SL, Stratford PW. Pharmacokinetic and safety study of doxorubicin-eluting beads in a porcine model of hepatic arterial embolization. J Vasc Interv Radiol. 2006; 17(8):1335–1343. [PubMed: 16923981]

28. Deschamps F, Solomon SB, Thornton RH, et al. Computed Analysis of Three-Dimensional Cone-Beam Computed Tomography Angiography for Determination of Tumor-Feeding Vessels During Chemoembolization of Liver Tumor: A Pilot Study. Cardiovasc Intervent Radiol. 2010

29. Loffroy R, Lin M, Rao P, et al. Comparing the Detectability of Hepatocellular Carcinoma by C-Arm Dual-Phase Cone-Beam Computed Tomography During Hepatic Arteriography With Conventional Contrast-Enhanced Magnetic Resonance Imaging. Cardiovasc Intervent Radiol. 2011

30. Wallace MJ, Kuo MD, Glaiberman C, Binkert CA, Orth RC, Soulez G. Three-dimensional C-arm cone-beam CT: applications in the interventional suite. J Vasc Interv Radiol. 2009; 20(7 Suppl):S523–S537. [PubMed: 19560037]

31. Virmani S, Wang D, Harris KR, et al. Comparison of transcatheter intraarterial perfusion MR imaging and fluorescent microsphere perfusion measurements during transcatheter arterial embolization of rabbit liver tumors. J Vasc Interv Radiol. 2007; 18(10):1280–1286. [PubMed: 17911519]

32. Dreher MR, Chilkoti A. Toward a systems engineering approach to cancer drug delivery. J Natl Cancer Inst. 2007; 99(13):983–985. [PubMed: 17596569]
33. Kennedy AS, Salem R. Radioembolization (yttrium-90 microspheres) for primary and metastatic hepatic malignancies. Cancer J. 2010; 16(2):163–175. [PubMed: 20404614]
34. Bonomo G, Pedicini V, Monfardini L, et al. Bland embolization in patients with unresectable hepatocellular carcinoma using precise, tightly size-calibrated, anti-inflammatory microparticles: first clinical experience and one-year follow-up. Cardiovasc Intervent Radiol. 2010; 33(3):552–559. [PubMed: 19957182]
35. Fukumura D, Yuan F, Monsky WL, Chen Y, Jain RK. Effect of host microenvironment on the microcirculation of human colon adenocarcinoma. Am J Pathol. 1997; 151(3):679–688. [PubMed: 9284816]
36. Brown KT. Fatal pulmonary complications after arterial embolization with 40–120- micro m tris-acryl gelatin microspheres. J Vasc Interv Radiol. 2004; 15(2 Pt 1):197–200. [PubMed: 14963189]
37. Malagari K, Pomoni M, Kelekis A, et al. Prospective randomized comparison of chemoembolization with doxorubicin-eluting beads and bland embolization with BeadBlock for hepatocellular carcinoma. Cardiovasc Intervent Radiol. 2010; 33(3):541–551. [PubMed: 19937027]
38. Virmani S, Harris KR, Szolc-Kowalska B, et al. Comparison of two different methods for inoculating VX2 tumors in rabbit livers and hind limbs. J Vasc Interv Radiol. 2008; 19(6):931–936. [PubMed: 18503910]
39. Chen JH, Lin YC, Huang YS, Chen TJ, Lin WY, Han KW. Induction of VX2 carcinoma in rabbit liver: comparison of two inoculation methods. Lab Anim. 2004; 38(1):79–84. [PubMed: 14979992]
40. Lee KH, Liapi E, Buijs M, et al. Percutaneous US-guided implantation of Vx-2 carcinoma into rabbit liver: a comparison with open surgical method. J Surg Res. 2009; 155(1):94–99. [PubMed: 19181344]

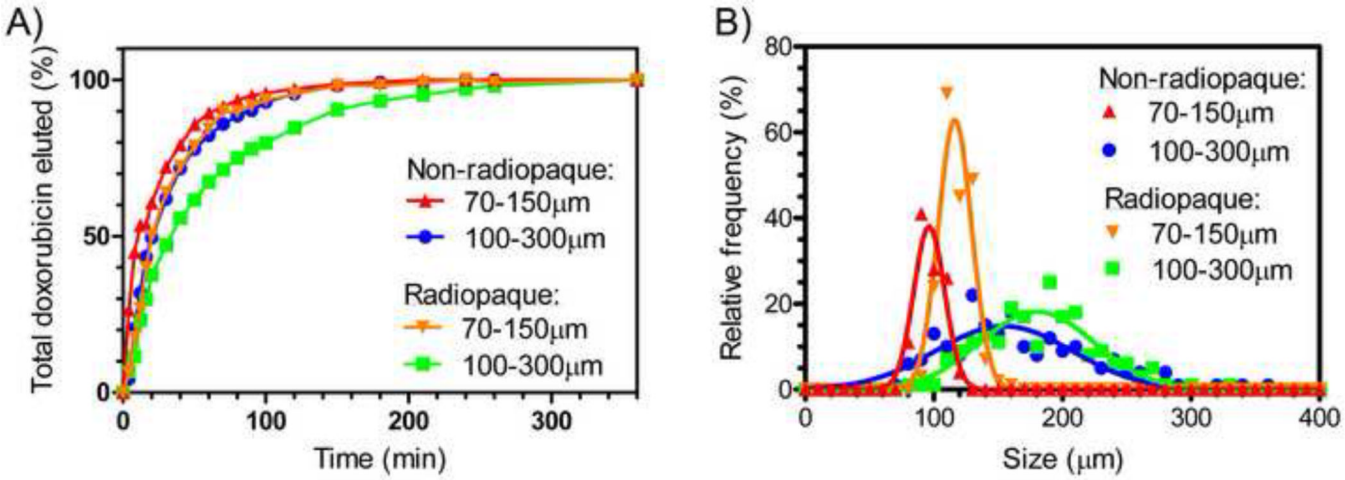

Figure 1.
Elution of doxorubicin (A) and size (B) of radiopaque beads and non-radiopaque beads.

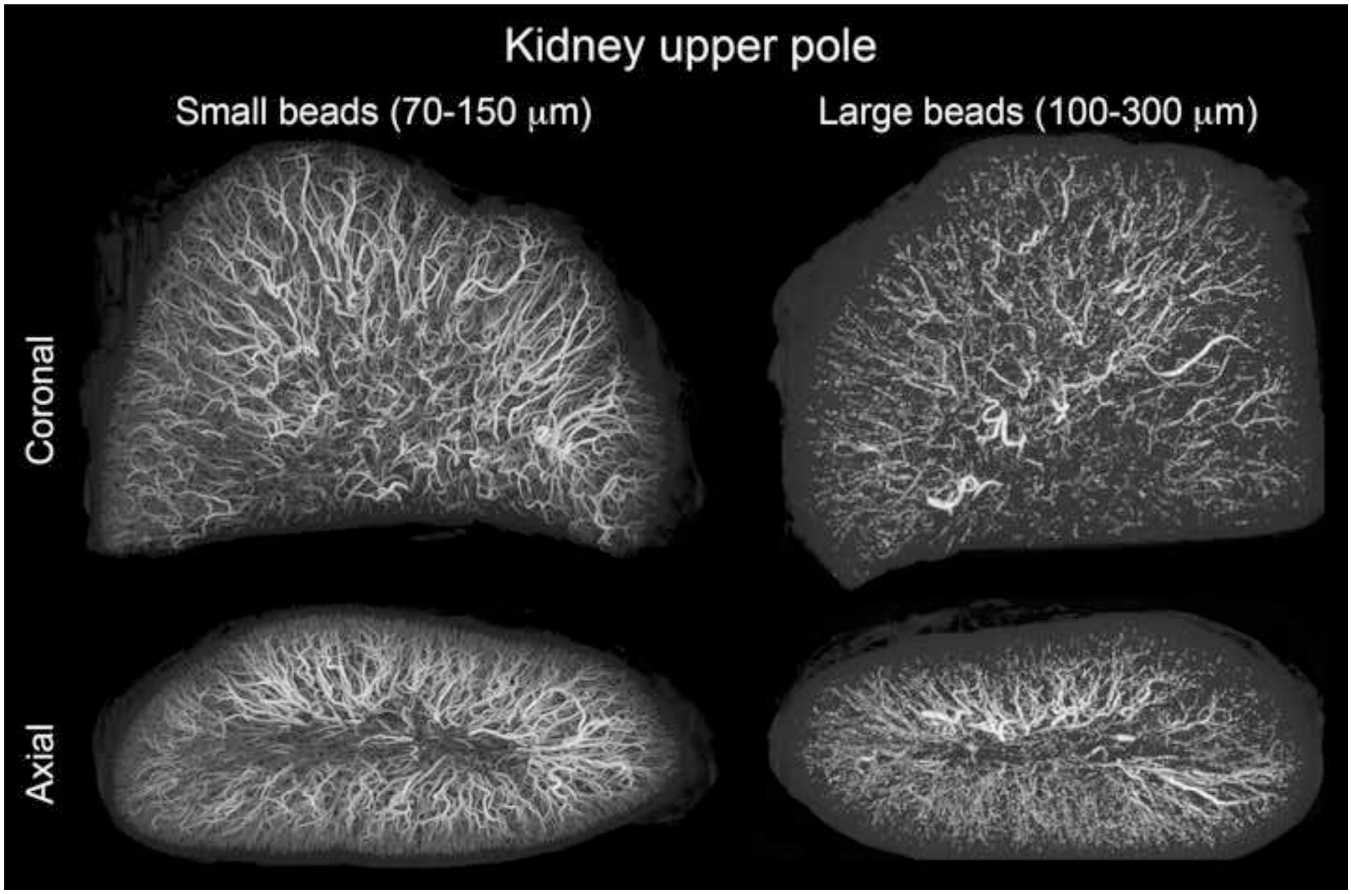

Figure 2.
microCT of swine kidney tissue embolized with radiopaque drug-eluting beads. Small (70–150 μm) and large (100–300μm) beads are displayed with consistent size scaling. Small beads penetrate to more distal regions and yield a greater spatial density.

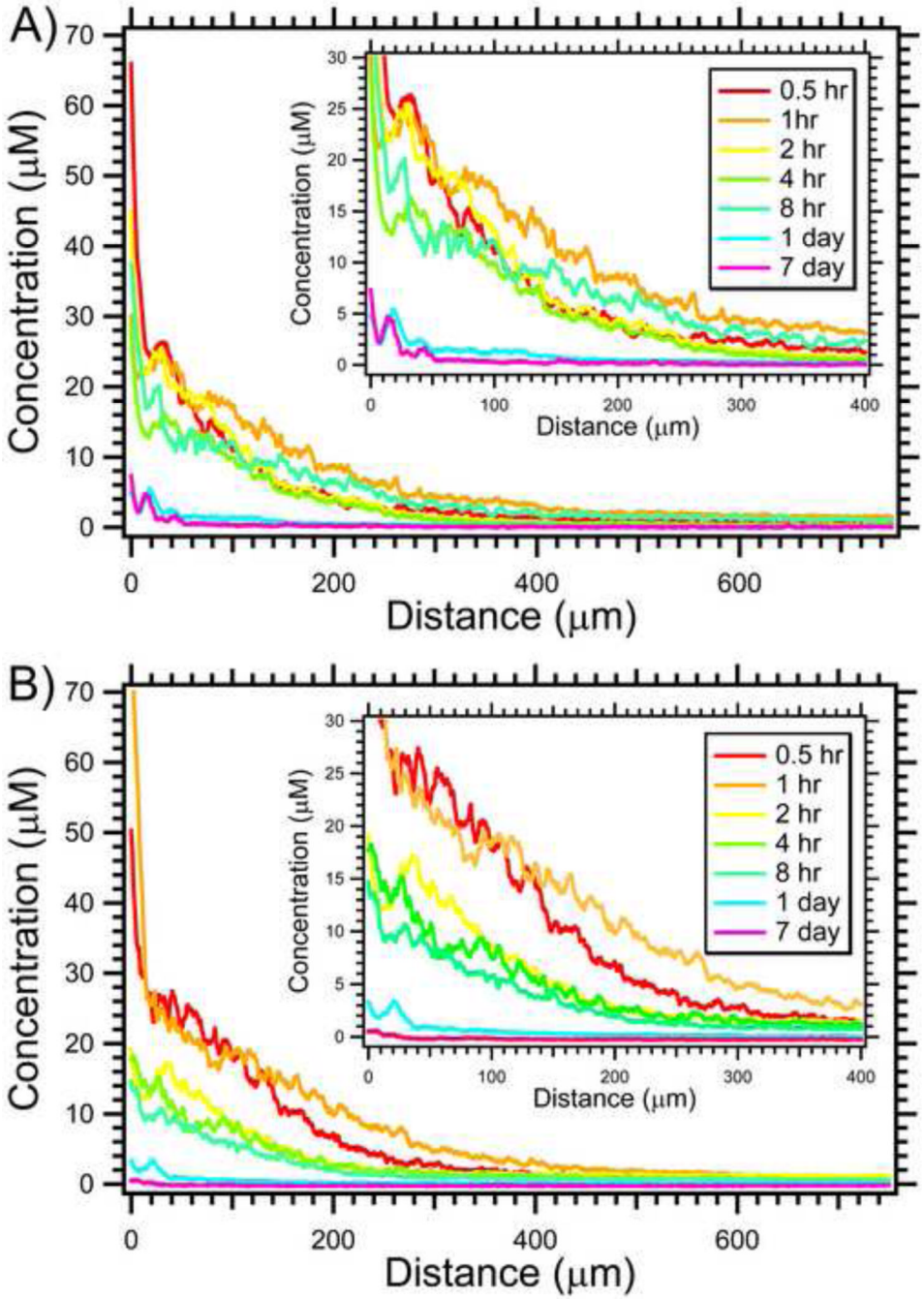

Figure 3.

Penetration of doxorubicin in swine liver for small 70–150μm (A) and large 100–300 μm (B) radiopaque drug-eluting beads. Insert displays a magnified view of the same data to better appreciate differences (N = 14–36).

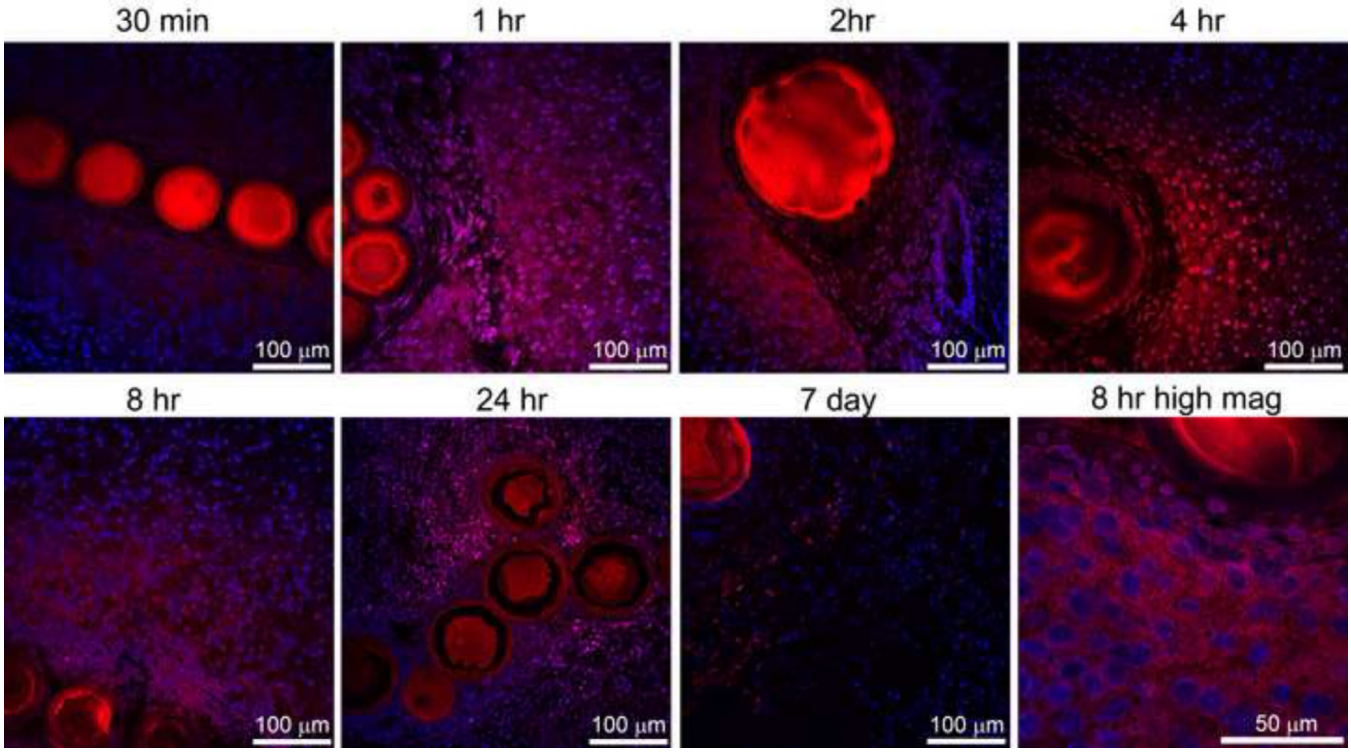

Figure 4.
Doxorubicin distribution surrounding radiopaque drug eluting beads with confocal microscopy. Doxorubicin (red) and nuclei (blue) levels were adjusted to best appreciate the distribution. All images are identical magnification with 100 μm bar except for the higher magnification image at 8 hr included in lower right panel (bar = 50 μm). Both 70–150μm and 100–300 μm radiopaque drug-eluting beads are included in this figure.

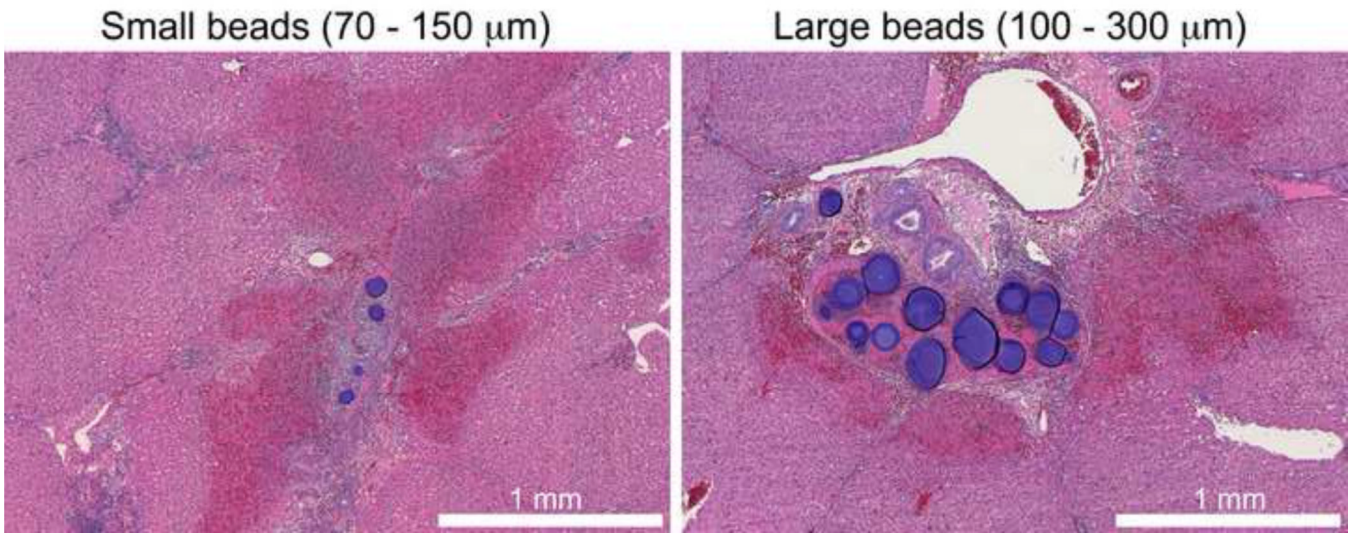

Figure 5.
Hematoxylin and eosin stain of swine liver tissue 24hr following transcatheter chemoembolization with radiopaque drug-eluting beads. Necrosis (indicated by light pink/red hue, eosinophilic appearance) is visible adjacent to the beads.